Acta Geochim (2022) 41(2):197–207
https://doi.org/10.1007/s11631-021-00505-y

ORIGINAL ARTICLE

Timing of granite pegmatite-type high-purity quartz deposit in the Eastern Qinling, China: constraints from in-situ LA-ICP-MS trace analyses of quartz and monazite U–Pb dating

Yong Zhang[1,3] · Haibo Zhao[2,4] · Lei Liu[2] · Jiayong Pan[1] · Likuan Zhu[2] · Guoqi Liu[1] · Xiaotian Zhang[1]

Received: 14 August 2021 / Revised: 9 October 2021 / Accepted: 18 October 2021 / Published online: 29 November 2021

Abstract Eastern Qinling, China is one of the important rare metal metallogenic provinces with extensively distributed granite pegmatite dikes. The No. 5 granite pegmatite intruded into the granitic gneiss of the Qinling Group, and the major minerals are quartz (39.8%), K-feldspar (18.8%), albite (36.3%), muscovite (3.4%), and garnet (1.1%). Monazite U–Pb isotopic dating indicates that the No. 5 pegmatite from the Eastern Qinling was emplaced at ca. 420.2 ± 2.2 Ma, which confirms that high-purity quartz mineralization probably formed during the Early Devonian. In-situ laser ablation inductively coupled plasma mass spectrometry analysis of quartz show that quartz samples from Eastern Qinling have total trace element concentrations (Al, Ti, Sc, Li, B, Cr, Mn, and Fe) ranging from 23.2 to 52.8 ppm, slightly higher than the quartz (impurity element content from 13.4 to 25.9 ppm) of the Spruce Pine high-purity quartz deposit in western North Carolina. The No. 5 pegmatite of Eastern Qinling could be defined as one high-purity quartz deposit of China.

✉ Yong Zhang
zhycy2004@163.com; zhangyong@ecut.edu.cn

✉ Haibo Zhao
tiger_zhaohb@163.com

[1] State Key Laboratory of Nuclear Resources and Environment (East China University of Technology), Nanchang 330013, China

[2] Zhengzhou Institute of Multipurpose Utilization of Mineral Resources, CAGS, Zhengzhou 450006, China

[3] Institute of Geological Survey of East China University of Technology, Nanchang 330013, China

[4] Xining Center of Natural Resources Comprehensive Survey, CGS, Xining 810000, China

Keywords Monazite · LA-ICP-MS · U–Pb · High-purity quartz · Granite pegmatite · Eastern Qinling

1 Introduction

Quartz is one of the most important rock-forming minerals of the Earth's crust and is an important industrial raw material (Götze et al. 2017). Naturally occurring high-purity quartz is in increasing demand due to emerging applications in the production of high-tech components such as optical fibers, halogen lamps, silica glass crucibles, computer chips, and solar panels (Müller et al. 2015). At present, the reserves of quartz vein deposits currently exploited in China are silica reserves from the 1950s to 1960s, of which the reserves of crystal quartz related to the production of high-purity quartz are nearly exhausted. China's "Medium–high grade" high-purity quartz (impurity element content lower 100 ppm) completely depends on imports. Unimin company of the United States occupies the "high grade" high-purity quartz (lower 30 ppm) produced in the world, and the origin is the Spruce Pine granite pegmatite metallogenic province of the United States. The study of Mineralogy and diagenetic age characteristics of granite pegmatite of high-purity quartz deposit may be one of the basic geological research tasks of high-purity quartz prospecting breakthrough in China.

Knowledge of the interrelation between quartz genesis and specific physical–chemical properties developed at that time can be used both for the reconstruction of geological processes and for specific technical applications (Götze 2009). Trace elements geochemistry of hydrothermal quartz which can precipitate from fluids with a wide range of compositions and temperatures, which enables it to

record the physicochemical history of the mineral systems (Peterková and Dolejš 2019; Rusk 2012; Rusk et al. 2008; Zhang et al. 2019b). Trace elements Li, Ge, Al, and Ti in quartz are the most common trace elements in magmatic quartz and their concentrations can be utilized to determine the degree of melt fractionation and the crystallization temperature of pegmatite applying the Ti-in-quartz geothermometer (Müller and Ihlen 2012). High-purity quartz contains trace elements (impurities) less than 500 ppm of contaminating (Götze et al. 2017; Larsen et al. 2000; Müller et al. 2007). The products of ultra-pure (high-purity) quartz are widely utilized in modern high-tech applications, such as optical fibers, semiconductors for the electronic industry, production of silicon cells for use in photovoltaic systems, as well as in industrial catalytic chemistry for the synthesis of catalysts, zeolites and adsorbent materials in general (Vatalis et al. 2015). The trace element chemistry of quartz is of crucial importance in defining the characteristics and geologic environments of high-purity quartz deposits (Müller et al. 2015). Impurities in quartz are the main controls on high-purity quartz quality as they can only be partly removed during processing (Götze and Möckel 2012). Lattice-bound trace elements are the most problematic, as they cannot currently be removed or reduced by processing (Müller et al. 2015). Therefore, the geological background, material source, controlling factors, and geological processes are the most important reason for the formation of high-purity quartz deposits.

The Eastern Qinling belt of the North Qinling terrane is one of the important granite pegmatite distribution region and rare metal metallogenic provinces, where extensively crop out granite pegmatite formed four pegmatite concentration zones (Lu et al. 2010). Quartz produce from a type of granite pegmatite has trace element contents lower than 65 ppm after an industrial mineral separation experiment by the Zhengzhou Institute of Multipurpose Utilization of Mineral Resources, China. However, the timing of granite pegmatite-type high-purity quartz mineralization at Eastern Qinling remains unclear. The zircon in pegmatite of the Eastern Qinling has undergone either before metamorphism or recrystallization, the cathodoluminescence image is black without obvious zoning (Wang et al. 2020), indicating that the U-Th system has been changed (Pei et al. 2015). Due to the loss of the Pb element in metamorphosed (ruditaceous) zircons, their ages are mostly scattered and their reliability is low. In contrast, monazite, a common mineral in peraluminous granite and pegmatite, has extremely high U, Th concentration, low common Pb, and high closure temperature of U-Th-Pb system, so that its crystallization ages can remain through a long history of geological events (Meldrum et al. 1998; Parrish 1990; Williams et al. 2007).

In this study, we combined detailed data of granite pegmatite geology, mineralogy, back-scanning electric (BSE) imaging, and in-situ LA-ICP-MS analyses of trace elements (impurity elements) of quartz and U–Pb isotopic of monazite from the No. 5 granite pegmatite high-purity quartz deposit in the Eastern Qinling, China. This study aims to compare the trace elements in granite pegmatite quartz of the Eastern Qinling and the Spruce Pine Mining District for a better understanding of the significance and geochronology of granite pegmatite events that formed high-purity quartz at Eastern Qinling. Furthermore, a genetic model will be established, which can be used both for the reconstruction of geological processes and for the metallogenic prediction of high-purity quartz deposits.

2 Geological background

The Qinling Orogen lies at the junction between the North and South China blocks, which preserves a record of Late Mid-Proterozoic to Cenozoic tectonism in central China (Meng and Zhang 2000; Ratschbacher et al. 2003). The Qinling Orogen is separated by the Shangdan Suture Zone into the North Qinling and South Qinling terranes (Fig. 1a) (Dong et al. 2011; Ratschbacher et al. 2003). The Qinling Orogen experienced a prolonged continental divergence and convergence between blocks (Meng and Zhang 2000). (1) The Proto-Tethyan Qinling Ocean stage from Late Neoproterozoic to Early Paleozoic. (2) The slab subduction stage during Ordovician. (3) The collision stage of South and North Qinling in Middle Paleozoic along the Shangdan suture. (4) The synchronous collision during the Late Paleozoic, resulting in the splitting of the South China block from the South Qinling. (5) The collision of the South Qinling and the South China block came about in the Late Triassic.

The North Qinling terrane is generally, from north to south, divided into the Kuanping, Erlangping, and North Qinling (or Qinling Group) units (Fig. 1b) (Ratschbacher et al. 2003; Zhai et al. 1998). The North Qinling unit consists of Precambrian garnet-bearing biotite–plagioclase gneisses, garnet–sillimanite gneisses, amphibolites, and marbles (Meng and Zhang 2000; Ratschbacher et al. 2003), all of which are intruded by Silurian–Devonian granitoids (Wang et al. 2009; Zhang et al. 2013). Neoproterozoic magmatism includes syn- to post-tectonic S-type granitoids and metabasaltic rocks (Chen et al. 2006; Shi et al. 2009). The Silurian–Devonian magmatic was characterized by the formation of arc-related I- and S-type granitoids (Wang et al. 2009; Zhang et al. 2013). Previously published U–Pb ages for these plutons range from 470 to 400 Ma (Li et al. 2019; Qin et al. 2014, 2015; Wang et al. 2017, 2009).

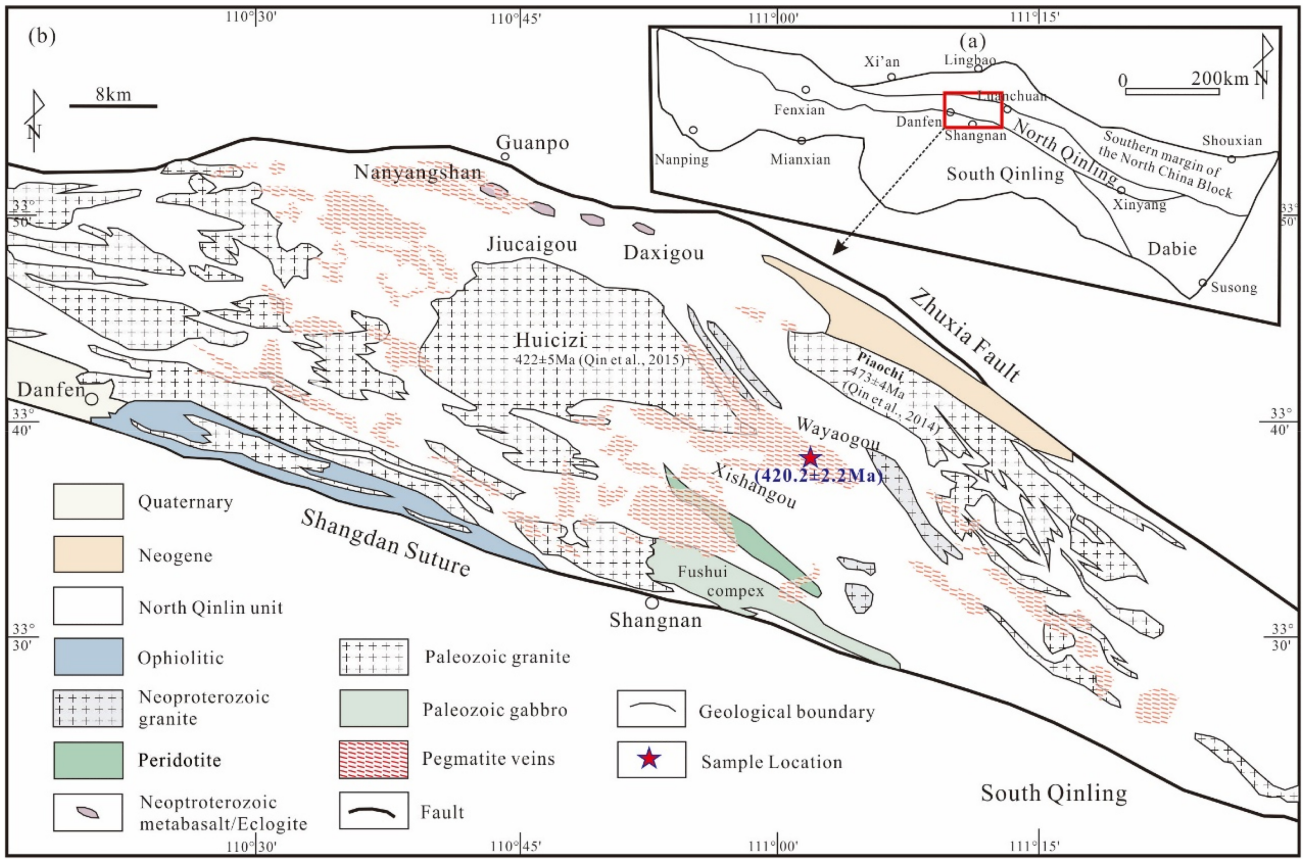

Fig. 1 Geological sketch of the Eastern Qinling terrane, modified after (Lu et al. 2010; Qin et al. 2014, 2015; Zhang et al. 2013; Zhou et al. 2019)

The Huichizi granites pluton in the North Qinling unit has high Sr/Y and (La/Yb)N ratios, and relatively high SiO_2, K_2O, and Na_2O, and very low MgO, Cr, and Ni contents similar to adakites(Qin et al. 2015). New SIMS zircon U–Pb dating constrains the emplacement age of the Huichizi pluton at 422 ± 5 Ma (Qin et al. 2015) (Fig. 1b). The Paleozoic Piaochi granitic intrusion is a large S-type peraluminous intrusion located in the North Qinling orogeny, emplaced at 473 ± 4 Ma (Qin et al. 2014) (Fig. 1b).

There are 6913 granite pegmatite dikes in the East Qinling, with the distribution of four concentrated areas, the Shangnan, Luanzhuang, guanpo, and longquanping (Lu et al. 2010) (Fig. 1b). The East Qinling granite pegmatite is mainly distributed in the granitic gneiss of the Paleoproterozoic Qinling group, and a small part is exposed in various metamorphic mafic rocks (pyroxenite, gabbro, etc.) of the Qinling group (Lu et al. 2010). Pegmatite dikes are 100-1000 m in length, generally 1–5 m in thickness. The occurrence of pegmatite dikes is steep with a dip angle of about 60°, which are banded around Caledonian huichizi, Taoping, and luoziping biotite monzogranite (Lu et al. 2010). As a rare metal and REE metallogenic province, pegmatite-type uranium deposit is also the most important uranium deposit of the eastern Qinling in central China (Chen et al. 2019; Wang et al. 2020; Zhang et al. 2017, 2019a).

The No. 5 granite pegmatite of the Eastern Qinling is a two-mica microcline pegmatite according to the classic classification of Lu et al (2010). The No. 5 granite pegmatite is about 300 m long and 50 m wide, which intruded into the granitic gneiss of the Qinling Group. The central phase of the No. 5 vein is a coarse-grained mica quartz-feldspar belt with a pegmatite structure (Fig. 2a), and the edge is a quartz-feldspar belt with granite structure (Fig. 2b). The main minerals are quartz (39.8%), potash feldspar (18.8%), albite (36.3%) (Fig. 2c), and muscovite (3.4%) (Fig. 2d, e), garnet (1.1%) after the scanning electron microscope-based Mineral Liberation Analyzer (SEM-MLA). The minor minerals are limonite (0.2%), apatite (0.1%), plagioclase (0.1%), calcite (0.08%), biotite (0.06%) (Fig. 2c, e), kaolinite (0.04%), ankerite (0.02%), uraninite (0.01%) and zircon (0.01%), and trace natural bismuth, rutile, dolomite, pyrite, phosphorite, etc. Pegmatites of the Spruce Pine Mining District in western North Carolina was a Medium fine-grained muscovite quartz feldspar granite (Fig. 2f, g, h).

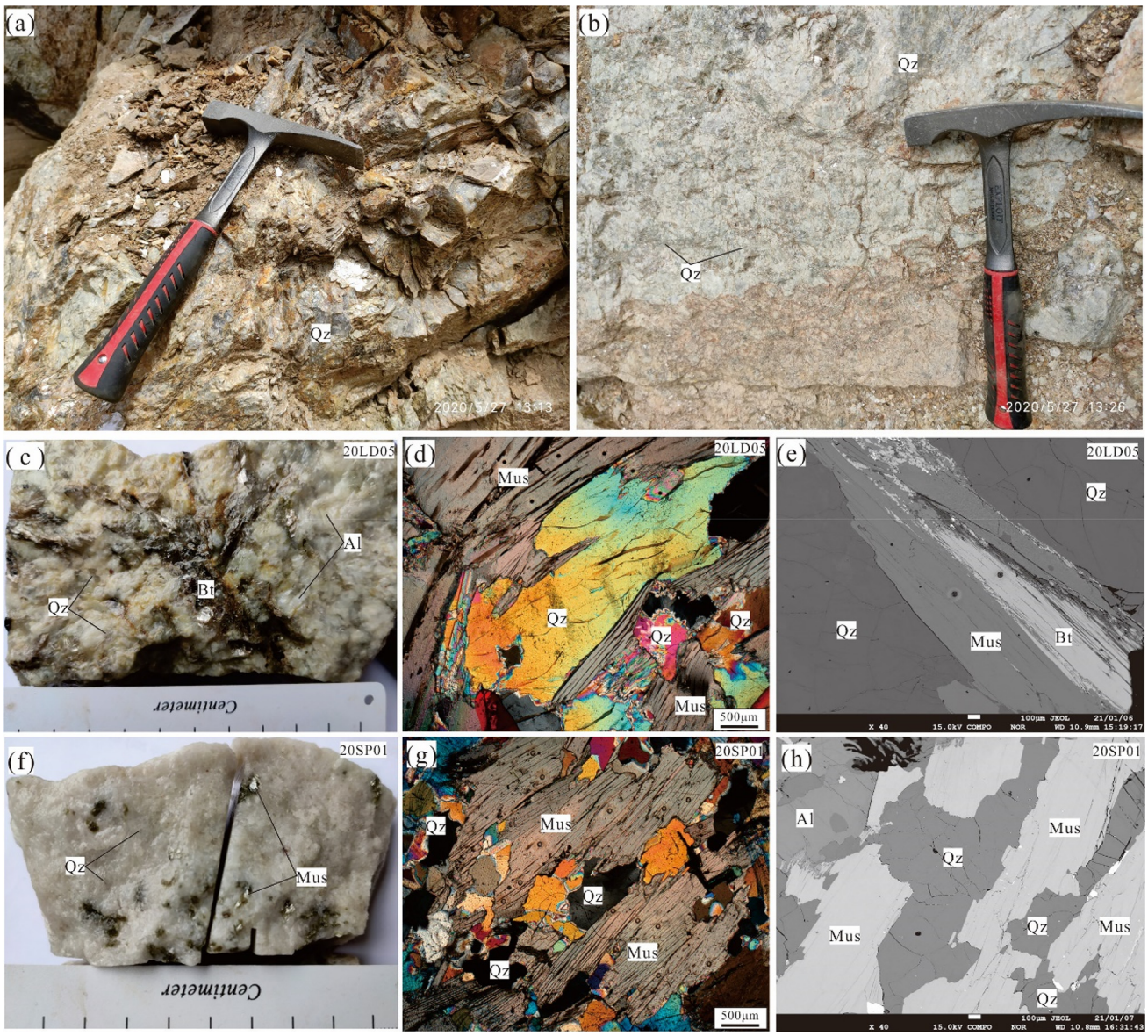

Fig. 2 Petrographic characteristics of No. 5 granite pegmatite in East Qinling and Spruce pine granite pegmatite from North Carolina

3 Sampling and analytical methods

3.1 Sampling

Geochronological work was performed on monazite, which is a common accessory mineral in the No. 5 granite pegmatite of the Eastern Qinling. Monazite of the No. 5 granite pegmatite preferentially incorporates high concentrations of Th and U while having very low initial concentrations of common Pb.

3.2 Analytical methods

(1) Electron backscatter

Quantitative chemical analyses and electron backscatter of the monazite samples were performed on polished thin sections using a JEOL JXA-8230 EMPA and ZEISS Gemini Sigma 300 VP at the State Key Laboratory of Nuclear Resources and Environment, East China University of Technology, China.

(2) LA-ICP-MS trace element analysis of quartz

The quartz trace element was performed by State Key Laboratory of Ore Deposit Geochemistry, Institute of Geochemistry, Chinese Academy of Sciences, Guiyang, China. Laser sampling was performed using a GeoLasPro 193 nm ArF excimer laser ablation system, coupled to an Agilent 7900 ICP–MS. A 44-μm spot was used with an energy density of 10 J/cm^2 and a repetition rate of 6 Hz. The instrument settings were optimized by ablating the NIST SRM 610 standard to obtain high signal intensities but a low oxide content (ThO/Th $< 0.3\%$) and doubly charged ion ($Ba^{2+}/Ba^{+} < 0.4\%$) production. Each LA–ICP–MS analysis incorporated a $\sim$15 s background acquisition (gas blank) and a 40 s data acquisition from each sample. Every thirteen-spot analysis was followed by two NIST SRM 610 analyses and one NIST SRM 612 to correct the time-dependent drift of sensitivity and mass discrimination of the ICP–MS. Reference glasses (NIST612 and NIST610) were analyzed before and after the sample measurements. The NIST SRM 610 was used as the external standard and data reduction was performed using the ICPMSDataCal software (Liu et al. 2008). Raw data reduction was performed offline with the ICPMSDataCal 10.1 software using the 100%-normalization strategy without applying an internal standard (Liu et al. 2008). The standard deviation of the trace elements was better than ± 10%.

(3) Monazite U–Pb ages

Geochronological analyses were performed was performed by FocuMS Technology Co. Ltd., Nanjing, China. Analyses were conducted on an Agilent 7700 × quadrupole inductively coupled plasma–mass spectrometer (ICP-MS) coupled with an ASI RESOlution S-155 laser-ablation system equipped with the TwoVol2 ablation cell using identical operating conditions. Laser ablation was performed using a 33 μm spot size, 8 Hz frequency, and 6.0 J/cm^2 fluence. Twenty-second-long background measurements were followed by a 40 s ablation time and 30 s washout. All isotopic data were normalized to the primary monazite reference material 44,069 (Aleinikoff et al. 2006), used as quality controls.

4 Results

4.1 Trace element of quartz

(1) Quartz from the Eastern Qinling

The Al and Ti, Sc, concentration in the quartz of the East Qinling ranged from 15.3 to 27.1 ppm and 2.2 to 3.7 ppm, 1.3 to 1.6 ppm, respectively (Table 1). While the Li, B, Cr, Mn, and Fe showed lower concentrations in the quartz at the East Qinling ranged from 0.0 to 0.1 ppm, 0.3 to 1.2 ppm, 0.0 to 2.9 ppm, 0.0 to 0.57 ppm, and 0.0 to 1.9 ppm, respectively (Table 1).

(2) Quartz from the Spruce Pine deposit

The Al and Ti, Sc concentration of the quartz of Spruce pine ranged from 8.3 to 19.6 ppm and 1.4 to 2.5 ppm, 0.9 to 1.1 ppm, respectively (Table 1). While the Li, B, Cr, Mn, and Fe showed lower concentrations of the quartz at the Spruce pine ranged from 0.0 to 0.07 ppm, 0.0 to 0.3 ppm, 0.3 ppm to 1.1 ppm, 0.0 to 0.8 ppm, and 0.0 to 2.5 ppm, respectively (Table 1).

4.2 In-situ U–Pb Isotopic dating on monazite

Sample 20LD05 was selected from No. 5 pegmatite for monazite U–Pb dating and the results were listed in Table 2. The monazite grains are generally prismatic, euhedral, transparent, and pale yellow. Their lengths mostly range from 80 to 180 μm with aspect ratios of 2:1 to 3:1(Fig. 3). Electron backscatter shows that the monazite is homogeneous. The grains have high uranium (87,580–106,611 ppm) and thorium (100,810–200,405 ppm) concentrations, and corresponding Th/U ratios of 1.39–2.54 (Table 2). Thirty-four analyses on monazite grains form a coherent group on the Concordia diagram, $^{206}Pb/^{238}U$ age range from 415 ± 13 Ma to 428 ± 14 Ma, yielding a weighted mean $^{206}Pb/^{238}U$ age of 420.2 ± 2.2 Ma (n = 34, MSWD = 0.31) (Table 2, Fig. 3).

5 Discussion

5.1 Potential high-purity quartz mineralization of the Eastern Qinling

High-purity quartz has become one of the strategically important resources with applications in high-tech industries including semiconductors, high-temperature lamp tubing, telecommunications and optics, microelectronics, and solar silicon applications (Dal Martello et al. 2012; Götze and Möckel 2012; Müller et al. 2015). Trace element concentrations in quartz from 188 granite pegmatites in the Froland and Evje-Iveland pegmatite fields, southern Norway, have been determined to establish exploration targets for high-purity quartz, which is unlikely to be of current economic interest due to its moderate to high trace element contents, heterogeneous compositions, and low volume (Müller et al. 2015). Quartz of different origins from 10 localities in the Southern Ural region, Russia, have been investigated to characterize their trace element compositions. The results show that almost all investigated quartz

Table 1 LA-ICP-MS trace element of quartz data for the granite pegmatite in East Qinling and Sprice pine (ppm)

Element	20LD05 (East Qinling)												
Li	0.022	0.014	0.014	–	0.103	0.084	0.033	0.006	0.013	0.054	–	–	0.033
Be	–	–	–	–	0.006	–	–	–	–	–	–	–	0.006
B	0.942	0.806	0.757	0.372	0.998	0.808	0.662	0.555	0.540	0.485	0.570	0.509	0.710
Mg	–	–	0.099	0.116	0.248	0.178	0.087	0.009	0.131	0.103	0.006	0.038	–
Al	21.325	24.433	20.057	20.149	27.098	24.045	22.421	15.307	24.579	21.959	20.368	22.199	24.696
Sc	1.536	1.555	1.561	1.535	1.540	1.582	1.555	1.532	1.399	1.516	1.369	1.450	1.378
Ti	3.258	2.812	2.230	2.412	3.012	2.487	2.611	2.329	3.454	3.442	2.503	2.386	2.368
Cr	0.227	0.292	0.052	0.780	0.527	0.688	–	0.425	2.885	1.023	0.008	0.561	0.372
Mn	–	0.385	–	–	0.187	–	–	0.361	0.559	0.434	–	–	–
Fe	1.898	0.073	–	0.361	–	–	0.538	–	–	–	–	0.329	–
Ge	1.441	2.322	1.831	1.832	1.737	1.925	1.737	2.344	1.517	1.974	1.940	2.376	1.960
Sn	0.632	0.557	0.450	0.516	0.360	0.524	0.536	0.347	0.466	0.341	0.300	0.365	0.357
total	31.3	33.2	27.0	28.1	35.8	32.3	30.2	23.2	35.5	31.3	27.1	30.2	31.9
Ge/Ti	0.4	0.8	0.8	0.8	0.6	0.8	0.7	1.0	0.4	0.6	0.8	1.0	0.8
Al/Ge	14.8	10.5	11.0	11.0	15.6	12.5	12.9	6.5	16.2	11.1	10.5	9.3	12.6
Al/Ti	6.5	8.7	9.0	8.4	9.0	9.7	8.6	6.6	7.1	6.4	8.1	9.3	10.4
T (°C)	454	445	432	436	449	438	441	434	458	458	439	436	435
Element	20LD05 (East Qinling)				20SP01 (Spruce pine)								
Li	–	–	–	–	0.069	0.060	–	0.005	0.051	0.006	0.034	–	–
Be	–	0.026	–	–	0.014	–	–	0.016	0.067	0.015	–	0.016	–
B	0.570	0.317	1.214	0.794	0.268	–	0.277	–	0.201	0.198	0.309	0.145	0.204
Mg	0.028	0.228	0.027	21.651	–	0.114	–	0.103	4.251	0.112	0.547	0.117	0.051
Al	20.045	20.097	23.221	22.345	9.934	9.897	8.922	10.325	12.509	8.300	19.571	9.132	12.114
Sc	1.416	1.307	1.383	1.271	1.029	1.058	0.956	1.046	0.964	0.925	0.975	0.956	0.948
Ti	2.196	2.726	3.378	3.670	2.091	1.851	1.374	1.805	2.400	2.308	2.183	2.494	1.886
Cr	0.082	0.301	1.004	0.219	0.340	0.801	0.565	1.089	0.734	0.741	0.835	0.356	0.576
Mn	0.209	–	0.570	0.135	0.171	–	0.012	–	0.305	0.830	–	–	–
Fe	–	–	1.006	0.550	–	2.393	–	–	0.948	0.050	0.199	1.613	2.498
Ge	1.916	1.426	1.528	1.673	1.165	1.086	1.132	1.059	1.300	1.303	1.130	0.818	1.434
Sn	0.289	0.199	0.395	0.477	0.201	0.204	0.143	0.266	0.113	0.190	0.125	0.138	0.159
total	26.8	26.6	33.7	52.8	15.3	17.5	13.4	15.7	23.8	15.0	25.9	15.8	19.9
Ge/Ti	0.9	0.5	0.5	0.5	0.6	0.6	0.8	0.6	0.5	0.6	0.5	0.3	0.8
Al/Ge	10.5	14.1	15.2	13.4	8.5	9.1	7.9	9.7	9.6	6.4	17.3	11.2	8.4
Al/Ti	9.1	7.4	6.9	6.1	4.8	5.3	6.5	5.7	5.2	3.6	9.0	3.7	6.4
T (°C)	431	444	456	462	428	421	405	420	436	434	431	438	422

"–" means under the detection limit. The ''TitaniQ'' thermometer of quartz calculate according to (Wark and Watson, 2006)

samples have very low concentrations of trace elements (Götze et al. 2017). Therefore, investigation of the concentration of impurities in quartz is the key to high purity quartz ore prospecting.

Using in-situ LA-ICP-MS analysis, we investigated the trace element composition of two types of high-purity quartz in pegmatite. Although all of the elements in quartz were detected, only the elements Li, Be, B, Na, Mg, Al, Ti, Sc, Ti, Cr, Mn, Fe, Ge, Sn have concentrations higher than the detection limit (Table 1). Total concentrations of trace elements (Total impurity elements) of quartz (23.2 to 52.8 ppm) from the No. 5 pegmatite are slightly higher than the quartz (13.4 to 25.9 ppm) from the Spruce Pine Mining District in western North Carolina. Impurity elements of quartz from the Eastern Qinling showed a similar pattern as Spruce Pine Mining (see Fig. 4). In addition, trace elements of quartz samples from Eastern Qinling are very low with cumulative concentrations less than 50 ppm,

Table 2 LA-ICP-MS Monazite U-Th-Pb isotopic data for the No. 5 pegmatite in East Qinling

No	ppm			Isotopic data						Ages (Ma)					
	Th	U	Th/U	$^{207}Pb/^{206}Pb$	1σ	$^{207}Pb/^{235}U$	1σ	$^{206}Pb/^{238}U$	1σ	$^{206}Pb/^{238}U$	1σ	$^{207}Pb/^{235}U$	1σ	$^{208}Pb/^{232}Th$	1σ
1	133677	87580	1.53	0.0542	0.0004	0.4968	0.0159	0.0665	0.0021	415	13	410	13	399	12
2	167509	92474	1.81	0.0540	0.0003	0.4993	0.0160	0.0671	0.0021	419	13	411	13	403	12
3	162542	94873	1.71	0.0540	0.0004	0.4966	0.0162	0.0667	0.0021	416	13	409	13	407	13
4	153272	83024	1.85	0.0545	0.0004	0.5038	0.0162	0.0671	0.0021	419	13	414	13	404	12
5	145921	95213	1.53	0.0540	0.0003	0.4951	0.0158	0.0664	0.0021	415	13	408	13	399	12
6	137513	88001	1.56	0.0542	0.0003	0.4965	0.0160	0.0665	0.0021	415	13	409	13	401	12
7	200405	90609	2.21	0.0537	0.0004	0.5008	0.0162	0.0676	0.0022	422	14	412	13	410	13
8	118915	90083	1.32	0.0534	0.0004	0.4957	0.0160	0.0673	0.0021	420	13	409	13	399	12
9	170033	77801	2.19	0.0535	0.0004	0.4947	0.0159	0.0671	0.0021	419	13	408	13	407	12
10	136016	82169	1.66	0.0538	0.0004	0.4984	0.0160	0.0672	0.0021	419	13	411	13	398	12
11	135471	96207	1.41	0.0536	0.0003	0.4966	0.0159	0.0672	0.0021	419	13	409	13	397	12
12	173204	113918	1.52	0.0540	0.0004	0.4998	0.0160	0.0672	0.0021	419	13	412	13	402	12
13	116743	80053	1.46	0.0543	0.0004	0.5151	0.0165	0.0688	0.0022	429	14	422	14	389	12
14	117163	101882	1.15	0.0536	0.0003	0.4945	0.0157	0.0669	0.0021	417	13	408	13	399	12
15	139081	106611	1.30	0.0537	0.0003	0.4978	0.0160	0.0673	0.0021	420	13	410	13	400	12
16	160505	101734	1.58	0.0540	0.0003	0.4989	0.0161	0.0670	0.0021	418	13	411	13	405	13
17	135753	76994	1.76	0.0536	0.0004	0.5010	0.0160	0.0678	0.0021	423	13	412	13	395	12
18	162121	90668	1.79	0.0535	0.0004	0.4994	0.0160	0.0677	0.0021	422	13	411	13	401	12
19	112426	102844	1.09	0.0532	0.0004	0.4912	0.0159	0.0669	0.0021	418	13	406	13	393	12
20	140198	105716	1.33	0.0536	0.0004	0.4959	0.0158	0.0671	0.0021	418	13	409	13	401	12
21	182142	85879	2.12	0.0534	0.0004	0.5032	0.0163	0.0684	0.0022	426	14	414	13	410	13
22	163628	86181	1.90	0.0530	0.0004	0.4939	0.0159	0.0676	0.0021	422	13	408	13	403	13
23	219239	86174	2.54	0.0534	0.0003	0.4994	0.0159	0.0678	0.0021	423	13	411	13	409	13
24	172137	87956	1.96	0.0527	0.0004	0.4990	0.0160	0.0686	0.0022	428	14	411	13	404	12
25	151597	98783	1.53	0.0534	0.0004	0.5048	0.0162	0.0686	0.0022	428	14	415	13	404	12
26	113228	74836	1.51	0.0529	0.0004	0.4960	0.0157	0.0679	0.0021	424	13	409	13	400	12
27	150821	99476	1.52	0.0534	0.0004	0.4953	0.0158	0.0673	0.0021	420	13	408	13	402	12
28	187918	84758	2.22	0.0535	0.0004	0.5024	0.0163	0.0681	0.0022	425	14	413	13	412	13
29	158340	77589	2.04	0.0531	0.0004	0.4888	0.0156	0.0668	0.0021	417	13	404	13	399	12
30	131969	72228	1.83	0.0533	0.0004	0.4973	0.0159	0.0677	0.0021	422	13	410	13	400	12
31	125541	71376	1.76	0.0535	0.0004	0.4926	0.0157	0.0668	0.0021	417	13	407	13	394	12
32	100810	71671	1.41	0.0535	0.0004	0.4962	0.0159	0.0673	0.0021	420	13	409	13	391	12
33	200218	91418	2.19	0.0530	0.0004	0.4935	0.0156	0.0675	0.0021	421	13	407	13	408	13
34	123694	88929	1.39	0.0531	0.0003	0.4882	0.0157	0.0666	0.0021	416	13	404	13	395	12

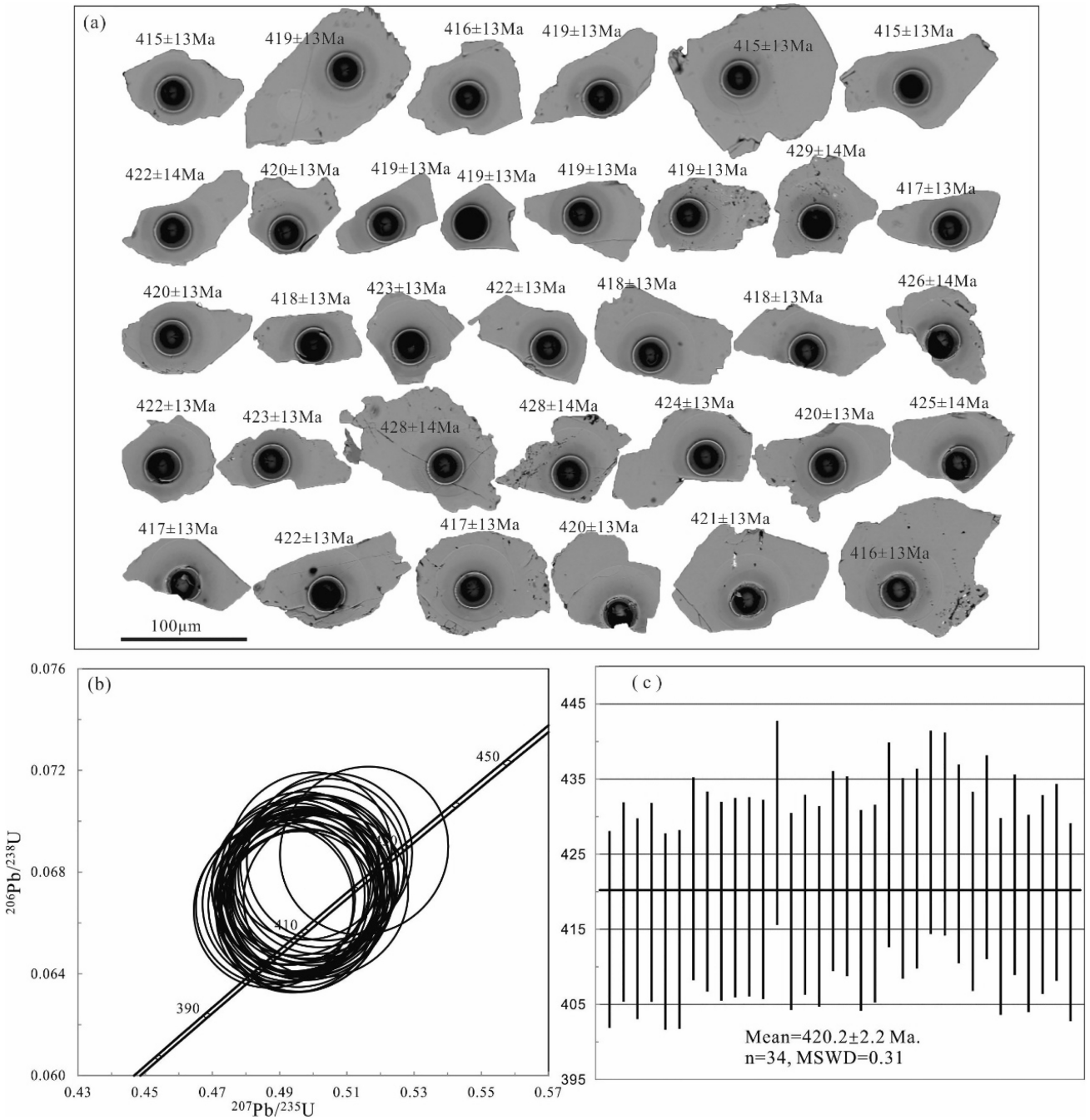

Fig. 3 Monazite U–Pb age dates for the sample from the No. 5 pegmatite in the East Qinling. **a** Electron backscatter of the Monazite and the $^{206}Pb/^{238}U$ age, **b** concordia diagram of the monazite (**c**). The weighted mean $^{206}Pb/^{238}U$ age of the granite pegmatite in the East Qinling

as Al < 30 ppm and Ti < 10 ppm, probably defining an economically high-purity quartz deposit of China.

5.2 Timing of high-purity quartz mineralization at the Eastern Qinling

Geological background, source of ore-forming materials, controlling factors, and other metallogenic theories have been thought to relate to the formation of high-purity quartz deposits. For example, the geological purification process model of high-purity quartz is the key basis for the breakthrough in prospecting and exploration of high-purity quartz deposits in China. Therefore, the geochronological setting constraint and comparison of the granite pegmatite-related high-purity quartz deposits from the Eastern

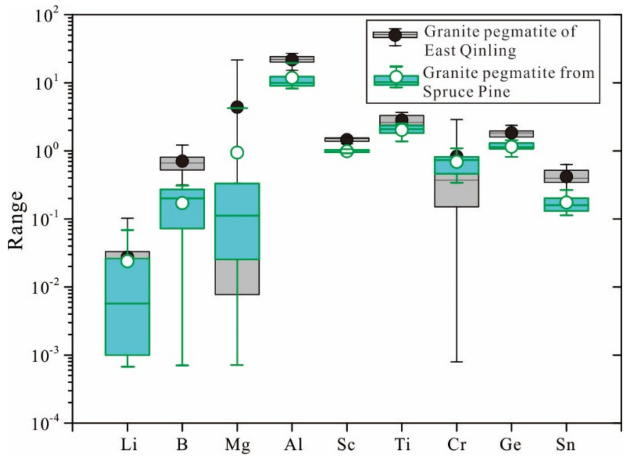

Fig. 4 LA-ICP-MS trace element of quartz from the No. 5 pegmatite and the Spruce Pine

Qinling and the Spruce Pine would make sense in understanding controls on the formation of this type of deposits.

Pegmatite of the Spruce Pine mining district in western North Carolina has a long history of providing various minerals to mankind (Borbst 1962; Glover 2012; Swanson and Veal 2010), which have the only magmatic high-purity quartz deposit in the world. The granodiorites of the Spruce Pine Plutonic Suite ages range from 377 fto 404 Ma (Swanson and Veal 2010). The Spruce Pine region shows high Na/K ratios, high large-ion lithophile elements Sr and Ba contents, low high-field strength and rare earth elements contents, positive Eu anomalies, formed with the interaction of mantle and crust (Zhang 2010).

The Qinling Orogen is located between the North China Block and South China Block and is linked with the Tongbai-Dabie orogens to the east and the Qilian-Kunlun orogens to the west (Zhang et al. 2013). The Paleozoic Piaochi granitic (Fig. 1) intrusion is a large S-type peraluminous intrusion in the North Qinling Orogen and has important implications for its tectonic evolution. SIMS and LA-ICPMS U–Pb zircon data obtained from magmatic zircons indicate that the Piaochi intrusion was emplaced at 473 ± 4 Ma (Qin et al. 2014). While SIMS zircon U–Pb dating constrains the emplacement age of the Huichizi pluton at 422 ± 5 Ma (Qin et al. 2015). The Huichizi pluton has relatively high SiO_2, K_2O, and Na_2O and very low MgO, Cr, and Ni contents, in the range of high-SiO_2 adakites. The whole-rock εNd(t) and zircon εHf(t) values of the Huichizi granite pegmatite are similar to the Neoproterozoic metabasalts in the North Qinling unit (Qin et al. 2015). In combination with their normal mantle-like $\delta^{18}O_{zircon}$ values, these adakites are thought to be produced by partial melting of the Neoproterozoic mafic crustal root due to subduction of the Shangdan Ocean (Qin et al. 2015).

Monazite U–Pb Isotopic dating indicates that the No. 5 pegmatite from the Eastern Qinling intrusion was emplaced at 420.2 ± 2.2 Ma (Fig. 3, Table 2). The emplacement age of the No. 5 quartz pegmatite is corresponding to the ages of the Huichizi pluton (422 ± 5 Ma) and Spruce Pine Plutonic Suite (377–404 Ma). Regional geological data of the North Qinling suggest that ca. 420 Ma is interpreted as the product of partial melting during the tectonic transition from compression to extension (Zhang et al. 2013). Geochronological of the No. 5 pegmatite and Spruce Pine high-purity quartz deposit shows that it is consistent in the error range. Consequently, monazite U–Pb isotopic dating confirms that high-purity quartz mineralization may form from a globally geological event of Early Devonian.

6 Conclusions

Trace-element analysis of quartz from the Eastern Qinling showed very low concentrations of trace elements (23.2 to 52.8 ppm), probably defining an economically high-purity quartz deposit.

In-situ monazite U–Pb dating indicates that the No. 5 pegmatite from the Eastern Qinling was emplaced at 420.2 ± 2.2 Ma, which confirms that high-purity quartz mineralization may form from a comparable geological event of Early Devonian.

Acknowledgements This research is funded by the National Natural Science Foundation of China (42062006 and 41962007), the National Key Research and Development Program of China (2016YFC0600207), the Project of China Geological Survey (DD20190186 and 12120114034501), and the science and technology research project of Jiangxi Provincial Department of Education(GJJ190379).

Authors' contributions Yong Zhang conceived of the presented idea and developed the theoretical formalism after wrote the manuscript. Hai-Bo Zhao provision of samples and preparation of regional geological maps. Lei Liu, Li-Kuan Zhu, Guo-Qi Liuand Xiao-Tian helped complete sample processing and testing. Jiayong Pan contributed to the final version of the manuscript.

Availability of data and materials The results from our study is our original unpublished work and it has not been submitted to any other journal for reviews.

Code availability There are no software application or custom code.

Declarations

Conflict of interest On behalf of all authors, the corresponding author states that there is no conflict of interest.

Ethics approval This manuscript we wish to be considered for publication in "ACTA Geochimica". No conflict of interest exits in the submission of this manuscript, and manuscript is approved by all authors for publication. I would like to declare on behalf of my co-

authors that the work described was original research that has not been published previously, and not under consideration for publication elsewhere, in whole or in part. All the authors listed have approved the manuscript that is enclosed.

Consent to participate We agree to participate in the arrangement of manuscript submission by the editorial department of the journal.

Consent for publication We agree to publish this manuscript.

References

Aleinikoff JN, Schenck WS, Plank MO, Srogi LA, Fanning CM, Kamo SL, Bosbyshell H (2006) Deciphering igneous and metamorphic events in high-grade rocks of the Wilmington complex, Delaware: morphology, cathodoluminescence, and backscattered electron zoning, and SHRIMP U-Pb geochronology of zircon and monazite. Geol Soc Am Bull 118(1–2):39–64

Borbst DA (1962) Geology of the Spruce Pine District, Avery, Mitchell, and Yancey Counties, North Carolina. Contributions to Economic Geology, pp 1–64

Chen ZH, Lu SN, Li HK, Li HM, Xiang ZQ, Zhou HY, Song B (2006) Constraining the role of the Qinling orogen in the assembly and break-up of Rodinia: tectonic implications for Neoproterozoic granite occurrences. J Asian Earth Sci 28(1):99–115

Chen YW, Hu RZ, Bi XW, Luo JC (2019) Genesis of the Guangshigou pegmatite-type uranium deposit in the North Qinling Orogenic Belt, China. Ore Geol Rev 115:103165

Dal Martello E, Bernardis S, Larsen R, Tranell G, Di Sabatino M, Arnberg L (2012) Electrical fragmentation as a novel route for the refinement of quartz raw materials for trace mineral impurities. Powder Technol 224:209–216

Dong Y, Zhang G, Neubauer F, Liu X, Genser J, Hauzenberger C (2011) Tectonic evolution of the Qinling orogen, China: review and synthesis. J Asian Earth Sci 41(3):213–237

Götze J (2009) Chemistry, textures and physical properties of quartz–geological interpretation and technical application. Mineral Mag 73(4):645–671

Götze J, Möckel R (2012) Quartz: Deposits, mineralogy and analytics. Springer, Berlin, pp 1–366

Götze J, Pan Y, Müller A, Kotova E, Cerin D (2017) Trace element compositions and defect structures of high-purity quartz from the southern Ural region. Russia Minerals 7(10):189

Glover A (2012) The Spruce Pine Mining District, a brief review of the history, geology and modern uses of the minerals mined in the Spruce Pine mining district, pp 1–4

Larsen RB, Polve M, Juve G (2000) Granite pegmatite quartz from Evje-Iveland: trace element chemistry and implications for the formation of high-purity quartz. Norges Geologiske Undersokelse 436:57–66

Li KW, Fang HB, Guo JG, Liu K, Wang XJ (2019) Petrogeochemistry, Zircon U-Pb dating and geological significance of two-mica granites from Wuduoshan granite in Nanzhao County. Eastern Qinling Mountains Earth Sci 44(1):123–134

Liu YS, Hu ZC, Gao S, Günther D, Xu J, Gao CG, Chen HH (2008) In situ analysis of major and trace elements of anhydrous minerals by LA-ICP-MS without applying an internal standard. Chem Geol 257(1):34–43

Lu XX, Zhu CH, Gu DM, Zhang HM, Wu M, Wu Y (2010) The main geological and metallogenic characteristics of granite pegmatite in Eastern Qinling Belt. Geol Rev 56(1):21–30

Müller A, Ihlen PM (2012) Trace elements of pegmatitic quartz and their regional distribution in two pegmatite fields of southern Norway. In: Proceedings of the 10th international congress for applied mineralogy (ICAM). Springer, Berlin, pp 445–451

Müller A, Ihlen PM, Wanvik JE, Flem B (2007) High-purity quartz mineralisation in kyanite quartzites, Norway. Miner Deposita 42(5):523–535

Müller A, Ihlen PM, Snook B, Larsen RB, Flem B, Bingen B, Williamson BJ (2015) The chemistry of quartz in granitic pegmatites of southern Norway: Petrogenetic and economic implications. Econ Geol 110(7):1737–1757

Meldrum A, Boatner LA, Weber WJ, Ewing RC (1998) Radiation damage in zircon and monazite. Geochim Cosmochim Acta 62(14):2509–2520

Meng Q-R, Zhang G-W (2000) Geologic framework and tectonic evolution of the Qinling orogen, central China. Tectonophysics 323(3):183–196

Parrish RR (1990) U-Pb dating of monazite and its application to geological problems. Can J Earth Sci 27(11):1431–1450

Pei XL, Shi Y, Liang B, Liu XJ, Ding HH, Zhu YH (2015) Genesis of the metamict zircons in the pegmatite from the Qinling Group(Complex) in the North Qinling Terrane. J Guilin Univ Technol 035(004):675–685

Peterková T, Dolejš D (2019) Magmatic-hydrothermal transition of Mo-W-mineralized granite-pegmatite-greisen system recorded by trace elements in quartz: Krupka district. Eastern Krušné Hory/erzgebirge Chem Geol 523:179–202

Qin Z-w, Wu Y-B, Wang H, Gao S, Zhu L-Q, Zhou L, Yang S-H (2014) Geochronology, geochemistry, and isotope compositions of Piaochi S-type granitic intrusion in the Qinling orogen, central China: petrogenesis and tectonic significance. Lithos 202–203:347–362

Qin ZW, Wu YB, Siebel W, Gao S, Wang H, Abdallsamed MIM, Zhang WX, Yang SH (2015) Genesis of adakitic granitoids by partial melting of thickened lower crust and its implications for early crustal growth: a case study from the Huichizi pluton, Qinling orogen, central China. Lithos 238:1–12

Ratschbacher L, Hacker BR, Calvert A, Webb LE, Grimmer JC, McWilliams MO, Ireland T, Dong S, Hu J (2003) Tectonics of the Qinling (Central China): tectonostratigraphy, geochronology, and deformation history. Tectonophysics 366(1):1–53

Rusk B (2012) Cathodoluminescent textures and trace elements in hydrothermal quartz. In: Quartz: deposits, mineralogy and analytics. Springer, Berlin, pp 307–329

Rusk BG, Lowers HA, Reed MH (2008) Trace elements in hydrothermal quartz: relationships to cathodoluminescent textures and insights into vein formation. Geology 36(7):547–550

Shi Y, Yu JH, Xu XS, Qiu JS, Chen LH (2009) Geochronology and geochemistry of the Qinling Group in the eastern Qinling Orogen. Acta Petrologica Sinica 25(10):2651–2670

Swanson SE, Veal WB (2010) Mineralogy and petrogenesis of pegmatites in the Spruce Pine District, North Carolina, USA. J Geosci 55(1):27–42

Vatalis KI, Charalambides G, Benetis NP (2015) Market of high purity quartz innovative applications. Procedia Econ Finance 24:734–742

Wang T, Wang XX, Tian W, Zhang CL, Li WP, Li S (2009) North Qinling Paleozoic granite associations and their variation in space and time: implications for orogenic processes in the orogens of central China. Sci China Ser D Earth Sci 52(9):1359–1384

Wang CM, Deng J, Bagas L, Wang Q (2017) Zircon Hf–isotopic mapping for understanding crustal architecture and metallogenesis in the Eastern Qinling Orogen. Gondwana Res 50:293–310

Wang JB, Hou XH, Li WH, Zhang L, Zhao YD, Chen HB, Li WH (2020) Metallogenic characteristics and metallogenic model of the pegmatite type uranium deposit in Danfeng area. Eastern Qinling Mount Earth Sci 45(1):61–71

Wark DA, Watson EB (2006) TitaniQ: a titanium-in-quartz geothermometer. Contrib Mineral Petrol 152(6):743–754

Williams ML, Jercinovic MJ, Hetherington CJ (2007) Microprobe monazite geochronology: understanding geologic processes by integrating composition and chronology. Annu Rev Earth Planet Sci 35(1):137–175

Zhai XM, Day HW, Hacker BR, You ZD (1998) Paleozoic metamorphism in the Qinling orogen, Tongbai Mountains, central China. Geology 26(4):371–374

Zhang Y (2010) The characters of the granitic pegmatites of the Spruce Pine region of the United States and the Altay region of Xinjiang and it. Najing University, Nanjing, pp 1–60

Zhang CL, Liu L, Wang T, Wang XX, Li L, Gong QF, Li XF (2013) Granitic magmatism related to Early Paleozoic continental collision in North Qinling. Chin Sci Bull 58(23):4405–4410

Zhang PP, Chen HK, Wen GD, Zhang TL, Mo HF, Sima XZ, Qu K, A LL, Yin QQ (2017) A study of geological features of granitic pegmatite-type uranium ore deposits on periphery of Huichizi granitic pluton in Lushi County, Henan Province. Mineral Depos 36(6):1425–1438

Zhang W, Chen WT, Gao J-F, Chen H-K, Li J-H (2019a) Two episodes of REE mineralization in the Qinling Orogenic Belt, Central China: in-situ U-Th-Pb dating of bastnäsite and monazite. Miner Deposita 54(8):1265–1280

Zhang Y, Cheng J, Tian J, Pan J, Sun S, Zhang L, Zhang S, Chu G, Zhao Y, Lai C (2019b) Texture and trace element geochemistry of quartz in skarn system: perspective from Jiguanzui Cu–Au skarn deposit, Eastern China. ORE Geol Rev 109:535–544

Zhou QF, Qin KZ, Tang DM, Wang CL, Ma LS (2019) Mineralogical characteristics and significance of beryl from the rare-element pegmatites in the Lushi County, East Qinling, China. Acta Petrologica Sinica 35(7):1999–2012